Statistical equilibrium predictions of jets and spots on Jupiter

Bruce Turkington[†], Andrew Majda[‡§], Kyle Haven[†], and Mark DiBattista[‡]

[†]Department of Mathematics and Statistics, University of Massachusetts, Amherst, MA 01003; and [‡]Courant Institute of Mathematical Sciences and Center for Atmosphere Ocean Science, New York University, New York, NY 10012

Contributed by Andrew Majda, August 24, 2001

An equilibrium statistical theory of coherent structures is applied to midlatitude bands in the northern and southern hemispheres of Jupiter. The theory imposes energy and circulation constraints on the large-scale motion and uses a prior distribution on potential vorticity fluctuations to parameterize the small-scale turbulent eddies. Nonlinearly stable coherent structures are computed by solving the constrained maximum entropy principle governing the equilibrium states of the statistical theory. The theoretical predictions are consistent with the observed large-scale features of the weather layer if and only if the prior distribution has anticyclonic skewness, meaning that intense anticyclones predominate at small scales. Then the computations show that anticyclonic vortices emerge at the latitudes of the Great Red Spot and the White Ovals in the southern band, whereas in the northern band no vortices form within the zonal jets. Recent observational data from the Galileo mission support the occurrence of intense small-scale anticyclonic forcing. The results suggest the possibility of using equilibrium statistical theory for inverse modeling of the small-scale characteristics of the Jovian atmosphere from observed features.

Prominent examples of long-lived large-scale vortices in geophysical flows are those observed on the Jovian planets, such as the Great Red Spot (GRS) on Jupiter (1–3). The emergence and persistence of such coherent structures at specific latitudes, such as 22.4°S for the GRS, in a background zonal shear flow that seems to violate all of the standard stability criteria (1) are a genuine puzzle needing a theoretical explanation. The present article contributes to such an explanation by using a recent equilibrium statistical theory (4–6) to predict the coherent structures in the weather layer of Jupiter. This statistical theory is based on a few judiciously chosen dynamical invariants and does not involve any detailed resolution of the fluid dynamics. An important input to the theory is therefore a prior probability distribution for the one-point statistics of the potential vorticity, which parameterizes the unresolved small-scale turbulent eddies that produce the large-scale coherent structures. Below it is demonstrated that the equilibrium states of the statistical theory simultaneously have three key properties:

(*i*) Coherent monopolar vortices, such as the GRS, emerge at the appropriate latitudes within the zonal mean velocity profile, such as the Limaye profile derived from Voyager data.

(*ii*) The coherent vortices are anticyclones if and only if the prior distribution on potential vorticity fluctuations has anticyclonic skewness.

(*iii*) All steady flows realized as equilibrium states are nonlinearly stable, including zonal shear flows that contain prograde and retrograde jets and embedded vortices.

Here the theory is developed for a one and one-half layer quasigeostrophic model, which yields the limiting behavior of a corresponding shallow-water model in a standard fashion (7, 8). The one and one-half layer model is commonly used to interpret the measurements of the Jovian atmosphere from spacecraft and other observations (1, 2), because its idealized vertical structure is comparable to the limited knowledge about the vertical structure of the Jovian planets. In the statistical theory based on this model, the choice of the prior distribution is a fundamental issue. An inverse modeling strategy is adopted here with respect to the prior distribution—the statistical properties of the small-scale eddies encoded in the prior distribution are inferred from a comparison of the large-scale features of predicted flows with observed flows. These small-scale properties can then be tested by physical arguments, numerical experiments, or independent observational data. The predictions of the statistical theory are computed here for a midlatitude band in the southern hemisphere of Jupiter, where there is an abundance of coherent vortices, and for a midlatitude band in the northern hemisphere, where there is a notable lack of large vortices.

There are several other equilibrium statistical theories of large-scale coherent structures (9–12) besides the theory adopted here (4, 5), each having different strengths and weaknesses (6) in its mathematical formulation and potential physical applications. One of the stated goals of these theories is to predict the GRS and other Jovian vortices (11, 13, 14). Although it is rather easy to invoke any of these theories to produce coherent monopole vortices resembling the GRS in variety of circumstances, the situation is akin to that of direct numerical simulation, where various models produce vortices of the desired kind in a range of physical regimes (1). To our knowledge, the work presented here is the first to incorporate the actual observational record for Jupiter into a statistical equilibrium theory and to predict coherent structures that are consistent with those observations and possess the properties *i*, *ii*, and *iii*. The following is the plan for the remainder of the article. First, the fluid dynamical model is introduced, and the statistical equilibrium theory is summarized. Then, the computed results for bands in the northern and southern hemispheres are presented and contrasted, followed by a brief concluding discussion.

The Dynamical Model

The basic dynamical equations model the shallow layer whose motion is visible to observations, but take into account the zonal flow in the underlying deep lower layer by including an effective zonal topography (1, 15). This is a one and one-half layer model, in which the upper and lower layers are assumed to have constant densities with lighter fluid overlying heavier fluid; the depth of the upper layer is small compared with the lower layer, and the steady zonal geostrophically balanced flow in the lower layer is unaffected by the flow in the upper layer. In dimensionless variables, the quasigeostrophic model is governed by the nonlinear advection equation

$$Q_t - Q_x\psi_y + Q_y\psi_x = 0, \qquad [1]$$

and the linear elliptic equation

$$Q = \psi_{xx} + \psi_{yy} - \lambda^{-2}(\psi - \psi_2) + \beta y, \qquad [2]$$

Abbreviation: GRS, Great Red Spot.

[§]To whom reprint requests should be addressed at: Samuel Morse Professor of Arts and Sciences, Courant Institute of Mathematical Sciences, New York University, 251 Mercer Street, New York, NY 10012. E-mail: jonjon@cims.nyu.edu.

 www.pnas.org/cgi/doi/10.1073/pnas.221449898

where $Q = Q(x,y,t)$ is the potential vorticity and $\psi = \psi(x,y,t)$ is the streamfunction or, equivalently, the normalized height perturbation for the upper layer. The positive parameters λ and β are the nondimensionalized Rossby deformation radius and gradient of the Coriolis parameter, respectively. The choice of λ, β, and the streamfunction $\psi_2(y)$ for the lower layer is discussed below. The velocity fields for the upper and lower layers are nondivergent, and are given by $(u,v) = (-\psi_y,\psi_x)$ and $(u_2,0) = (-\psi_{2,y},0)$, respectively.

For all computations below, the flow domain is the zonal channel.

$$D = \{(x,y):|x| < 2,\ |y| < 1\}.$$

The boundary conditions for flow in this channel are achieved by setting $\psi = 0$ on the walls $y = \pm 1$ and imposing periodicity in x.

The Equilibrium Statistical Theory

In the statistical theory, the potential vorticity field Q is viewed as a fine-grained field that is randomized by the governing microscopic dynamics (Eqs. **1** and **2**), and a corresponding macroscopic description is introduced to capture the coarse-grained structure of Q. In an appropriate continuum limit, the statistical theory is an exact local mean-field theory (11, 12), and the macroscopic description is furnished by a spatially localized probability distribution $P(x,y,dq)$ on the random microstate Q at each point (x,y). The macrostate characterized by the theory is the probability density, $\rho = \rho(x,y,q)$, of $P(x,y,dq)$ with respect to a given "prior distribution" $\Pi(dq)$ (4, 5); namely,

$$P(x,y,dq) = \rho(x,y,q)\Pi(dq). \qquad [3]$$

The spatially homogeneous prior distribution Π is chosen to model the statistical properties of the small-scale fluctuations of the potential vorticity. In the inverse modeling strategy adopted here, the choice of Π is tested *a posteriori* by comparing the macroscopic predictions of the theory with the large-scale properties of the observed flows. For this reason, it is worthwhile to carry out the statistical equilibrium calculations for an arbitrary prior distribution before making a definite choice.

The equilibrium macrostate ρ maximizes the relative entropy.

$$S(\rho) = -\int_D\int \rho \ln \rho\, dxdy\Pi(dq) \qquad [4]$$

over all macrostates satisfying the constraints

$$H(\rho) = \frac{1}{2}\int_D (\bar{\psi}_x^2 + \bar{\psi}_y^2 + \lambda^{-2}\bar{\psi}^2)dxdy = E,$$

$$C(\rho) = \int_D (\bar{\psi}_{xx} + \bar{\psi}_{yy} - \lambda^{-2}\bar{\psi})dxdy = \Gamma, \qquad [5]$$

which reflect the conservation of total energy and circulation by the dynamics in Eqs. **1** and **2**. In these constraints, $\bar{\psi}$ is determined by ρ via the coarse-grained potential vorticity

$$\bar{Q}(x,y) = \int q\rho(x,y,q)\Pi(dq)$$

$$= \bar{\psi}_{xx} + \bar{\psi}_{yy} - \lambda^{-2}(\bar{\psi} - \psi_2) + \beta y. \qquad [6]$$

The constrained entropy maximization leads to the local mean-field equation

$$\bar{Q} = \frac{\int qe^{(\theta\bar{\psi} - \gamma)q}\Pi(dq)}{\int e^{(\theta\bar{\psi} - \gamma)q}\Pi(dq)}. \qquad [7]$$

The parameters θ and γ are the Lagrange multipliers for the energy and circulation constraints in Eq. **5**, respectively, and play the role of the "inverse temperature" and "chemical potential." It is instructive to write Eq. **7** in its variational form,

$$\bar{Q} = G'(\theta\bar{\psi} - \gamma), \quad \text{where} \quad G(s) = \ln\int e^{sq}\Pi(dq) \qquad [8]$$

is the cumulant generating function for the probability distribution Π. The properties of the coherent structure determined by the solution to Eq. **8** depend on the prior distribution Π through the properties of the real function $G' = dG/ds$. From the elementary formulas for the mean, variance, and skewness of the prior distribution Π,

$$G'(0) = \int q\Pi(dq) = \langle Q\rangle,$$

$$G''(0) = \int [q - \langle Q\rangle]^2\Pi(dq) = \text{var } Q,$$

$$G'''(0) = \int [q - \langle Q\rangle]^3\Pi(dq) = \text{skew } Q(\text{var } Q)^{3/2},$$

it is evident that the principal contribution to the nonlinearity of Eq. **8** scales with skew Q. In view of the importance of skewness, an attractive choice of the prior distribution is the centered gamma distribution

$$\Pi_\varepsilon(dq) = |\varepsilon|^{-1}R(\varepsilon^{-1}[q + \varepsilon^{-1}];\ \varepsilon^{-2})dq, \qquad [9]$$

where $R(z;a) = \Gamma(a)^{-1}z^{a-1}e^{-z}$ $(z \geq 0)$, $R(z;a) = 0$ $(z < 0)$ denotes the standard gamma density. The scaling of Π_ε is chosen so that

$$\langle Q\rangle = 0, \quad \text{var } Q = 1, \quad \text{skew } Q = 2\varepsilon. \qquad [10]$$

Because $R(z;a)$ has the cumulant generating function $-a\ln(1 - s)$, the local mean-field Eq. **8** associated with the prior distribution (Eq. **9**) takes the explicit form

$$\bar{Q} = G'_\varepsilon(\theta\bar{\psi} - \gamma) = \frac{\theta\bar{\psi} - \gamma}{1 - \varepsilon(\theta\bar{\psi} - \gamma)}. \qquad [11]$$

In the limit as the skewness parameter $\varepsilon \to 0$, Π_ε converges to the standard Gaussian distribution, and the corresponding statistical equilibrium theory reduces to the standard energy–enstrophy theory (6, 9, 10).

In applying the equilibrium statistical theory formulated above, it is useful to adopt the viewpoint that the prior distribution Π_ε encodes the statistics of the potential vorticity fluctuations induced by small-scale forcing, and that the solution $\bar{Q}$ to Eq. **11** represents the large-scale structure resulting from an inverse cascade process. Such a perspective is confirmed in a variety of flow regimes for various idealized models by comparing crude closure schemes based on equilibrium statistical theory to direct numerical simulations with random small-scale forcing (16–18). This viewpoint contrasts with other numerical studies of equilibrium statistical theories that emphasize freely decaying turbulence (12, 19). A similar approach to prior distributions and

inverse cascades has been used by M.D. and A.M. in statistical models parameterizing open ocean deep convection (20, 21).

Application to Jets and Spots on Jupiter

First, it is necessary to fit the dimensionless parameters and fields in the dynamical equations in Eqs. **1** and **2** to their dimensional counterparts for the Jovian atmosphere, which are distinguished by asterisk superscripts. Let D^* be the flow domain that lies between the latitudes Θ_- and Θ_+, and let u^* be the zonally averaged velocity profile for this domain of Jupiter determined by Limaye (3, 22). A centered Limaye profile, $\tilde{u}^*$, obtained by subtracting from u^* its average over the domain, is introduced so that the zonal mean flow satisfies the boundary conditions $\tilde{\psi}^* = 0$ at the channel walls. With this adjustment of frame of reference, no constraint associated with the conservation of linear impulse is required in the constraints (Eq. **5**) for the maximum entropy principle. The characteristic length scale L is defined to be half the channel width, and the characteristic velocity scale U is defined to be the rms velocity of the centered Limaye profile; namely,

$$L = \frac{(\Theta_+ - \Theta_-)r_0}{2}, \quad U^2 = \frac{1}{2L}\int (\tilde{u}^*)^2 dy^*,$$

where $r_0 = 7 \times 10^7 m$ is used for the radius of the planet. The dimensional constants β^* and λ^* are computed from the Coriolis parameter $f(\Theta) = 2\Omega\sin\Theta$, with $\Omega = 1.76 \times 10^{-4}\ s^{-1}$, at the center latitude Θ_0 of the channel; specifically,

$$\beta^* = \frac{f'(\Theta_0)}{r_0}, \quad \lambda^* = \frac{c}{f(\Theta_0)},$$

where $c = 454 ms^{-1}$ is the estimated gravity wave speed for Jupiter (23). The dimensionless model parameters are then $\beta = L^2U^{-1}\beta^*$ and $\lambda = L^{-1}\lambda^*$. The fields Q and ψ are similarly nondimensionalized by L and U; in particular, the dimensionless centered Limaye streamfunction is

$$\tilde{\psi} = -\int_{-1}^{y} \tilde{u}(y')dy', \quad \text{with} \quad \tilde{u} = U^{-1}\tilde{u}^*.$$

There is no available data on the zonal velocity profile of the lower layer, and consequently there is no direct way to deduce ψ_2. Dowling (1, 23) has noted that a good fit for the observational data is obtained by imposing the linear relation

$$\tilde{Q} = \theta\tilde{\psi} - \gamma \quad \text{with} \quad \theta \approx -\lambda^{-2}. \qquad [12]$$

This relation combined with Eq. **2** then determines the effective zonal topography

$$\psi_2 = (\lambda^2\theta + 1)\tilde{\psi} + \lambda^2\left(\frac{d\tilde{u}}{dy} - \beta y - \gamma\right). \qquad [13]$$

In the computations presented here, the parameter θ in Eq. **13** is selected to be $\theta = -\lambda^{-2} - (\pi/2)^2$, the first eigenvalue of $\partial^2/\partial x^2 + \partial^2/\partial y^2 - \lambda^{-2}$ on D. When ψ_2 is fixed with this value, which is close to Dowling's approximate value, $\tilde{\psi}$ is a bifurcation point for the energy–enstrophy theory. Other selection criteria for θ are compatible with the analysis of observed data in refs. 1 and 23 and result in small changes in the effective zonal topography; those criteria will be discussed elsewhere. For any given value of θ, the parameter γ in Eq. **12** is chosen so that $\int_{-1}^{+1}\psi_2 dy = 0$.

Next, solutions to the constrained maximum entropy problem (Eqs. **4** and **5**) are computed by using the iterative algorithm developed in refs. 5 and 24. The zonal topography ψ_2 is determined by the Dowling procedure (Eq. **13**), and the constraint values E and Γ are derived from $\tilde{\psi}$. Consequently, the solution corresponding to $\varepsilon = 0$ is a zonal shear flow that coincides with the centered Limaye profile on the channel domain. Branches of solutions are therefore computed by varying the skewness parameter ε in the prior distribution (Eq. **9**), holding ψ_2, E, and Γ fixed. Because virtually all of the large coherent vortices on Jupiter have anticyclonic relative vorticity, it is natural to expect that they emerge as equilibrium states in a statistical theory with a prior distribution having anticyclonic skewness. This conjecture is tested for particular channel domains in the southern and the northern hemispheres. Each domain contains five alternating zonal jets of the Limaye profile and consists of two zones and two belts.

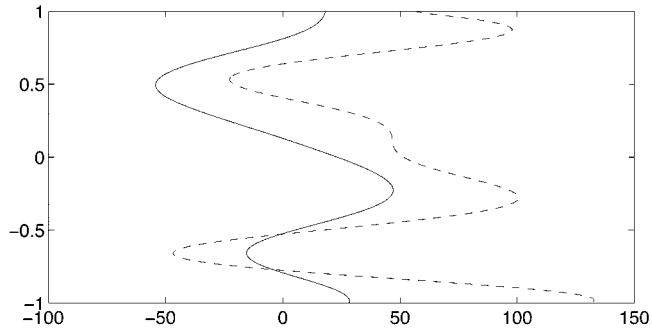

Fig. 1. The Limaye zonal mean velocity profile for the southern hemisphere band from 36.6°S and 13.7°S (solid), and the zonal velocity profile for the lower layer (dashed) inferred by the Dowling procedure.

The Southern Hemisphere Domain

The large-scale coherent structures predicted by the statistical equilibrium theory are computed for a channel domain between 36.6°S and 13.7°S in latitude. (For the sake of clarity, the usual northern hemisphere conventions are used in the discussion of southern hemisphere flows.) Fig. 1 displays the Limaye profile, u^*, for the upper layer together with velocity profile, u_2^*, for the lower layer determined by Eq. **13**. By construction, the computed solution, $\overline{u}^*$, for $\varepsilon = 0$ coincides with the centered Limaye profile, $\tilde{u}^*$. In this and the subsequent figures, the zonal profiles of computed equilibrium states are plotted with respect to the reference frame of the uncentered Limaye profile. The streamline plots displayed in Fig. 2 correspond to solutions with the same values of energy E and circulation Γ as in Fig. 1, but with anticyclonic skewness $\varepsilon = -0.02, -0.035$. These plots clearly show that a large coherent vortex forms in the zonal shear flow and becomes stronger and more concentrated as the skewness parameter increases. This large vortex is an anticyclone centered in latitude at ≈23°S, the latitude of the GRS. Furthermore, the vortex for $\varepsilon = -0.035$ has nearly the same size and shape as the GRS. A weaker anticyclonic vortex also forms south of the large vortex at 32°S, in the zone that corresponds to the location of the White Ovals. In the belt between those zones and in the belt north of the GRS, there are regions of recirculating cyclonic flow. All these predictions of the statistical equilibrium theory are consistent with the observed large-scale features of the Jovian southern hemisphere (3). In Fig. 3, the zonal mean-velocity profiles for the upper layer flows corresponding to $\varepsilon = -0.02, -0.035$ are plotted together with the Limaye profile. It is noteworthy that, even though the computed solution with $\varepsilon = -0.035$ contains a strong vortex, its zonally averaged profile departs only slightly from the Limaye profile.

The Northern Hemisphere Domain

In analogy to the southern hemisphere computation, the theory is applied to a channel domain from 23.1°N to 42.5°N in latitude.

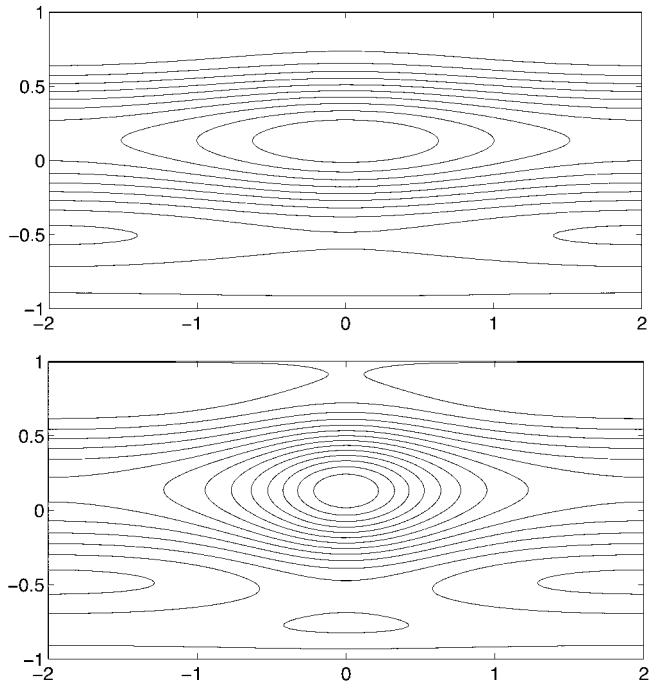

Fig. 2. Mean streamline plots for the equilibrium states over the effective zonal topography in Fig. 1, with skewness parameter $\varepsilon = -0.02$ (*Upper*) and $\varepsilon = -0.035$ (*Lower*), and the same energy and circulation as the Limaye zonal flow. The length scale is $L = 14{,}000$ km.

This implementation provides an interesting test of the theory because no large-scale coherent vortices are observed in this domain of Jupiter. Fig. 4, which is analogous to Fig. 1, displays the Limaye profile, u^*, and the zonal velocity profile, u_2^*, for the lower layer determined by Eq. **13**. The solutions corresponding to skewness parameter $\varepsilon = -0.02, -0.032$ and having the same energy and circulation as the Limaye solution with $\varepsilon = 0$ are then computed. In striking contrast to the southern hemisphere computation, these equilibrium states are purely zonal shear flows. The zonal velocity profiles for these solutions are plotted together in Fig. 5. In fact, all of the solutions corresponding to $0 > \varepsilon > -0.032$ are zonal, and for $\varepsilon < -0.033$ solutions fail to exist. Even though no coherent vortices emerge, it is evident from Fig. 5 that the zonal jet structure of these solutions is modified significantly as the anticyclonic skewness increases.

Nonlinear Stability

All of the steady-flow fields calculated in Figs. 1–5 are nonlinearly stable with respect to the dynamics of frictionless flow in the upper layer with fixed topography. In fact, all coherent structures identified with equilibrium states of the statistical theory enjoy this stability property. The nonlinear stability of these most probable states can be proved by constructing Lyapunov functionals from the objective and constraint functionals appearing in the maximum entropy principle (Eqs. **4** and **5**). This construction is related to the classical approach of Arnold (25), in which a Lyapunov functional for a given steady flow, such as a zonal shear flow, is defined by combining the energy functional with the generalized enstrophy functional associated with that steady flow. In the approach taken here, the role of the generalized enstrophy functional is played by the negative entropy, which can be expressed as a convex functional of the coarse-grained potential vorticity, $\overline{Q}$. The Lyapunov functional of Arnold is then identical with the Lagrangian for the constrained maximization problem (Eqs. **4** and **5**). In the Jovian applications considered here, however, the second variation of this Lagrangian is typically not positive-definite with respect to arbitrary variations, $\delta\overline{Q}$. Consequently, the Arnold sufficient conditions for stability fail in general, as has been noticed by Dowling (1, 23, 26). Nevertheless, for any equilibrium state $\overline{Q}$ of the statistical theory a Lyapunov functional whose second variation is positive-definite at $\overline{Q}$ can be constructed by forming the "augmented Lagrangian," a standard tool of optimization theory (27) for treating constrained problems. The key idea in this refined stability analysis is to account for the dynamical constraints (Eq. **5**) in the Lyapunov argument. A detailed discussion of this approach is given by B.T. and K.H. (28); its application to coherent structures in a Jovian atmosphere will be described elsewhere.

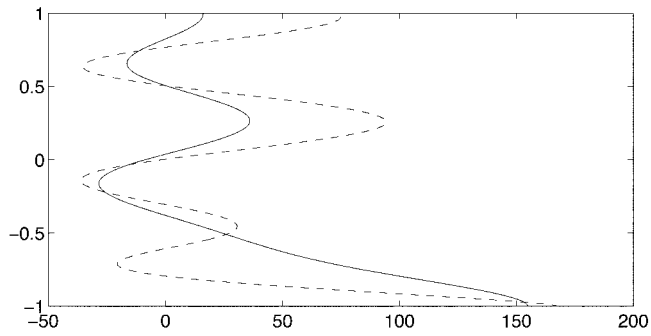

Fig. 4. The Limaye zonal mean velocity profile for the northern hemisphere band from 23.1°N to 42.5°N (solid), and the zonal velocity profile for the lower layer (dashed) inferred by the Dowling procedure.

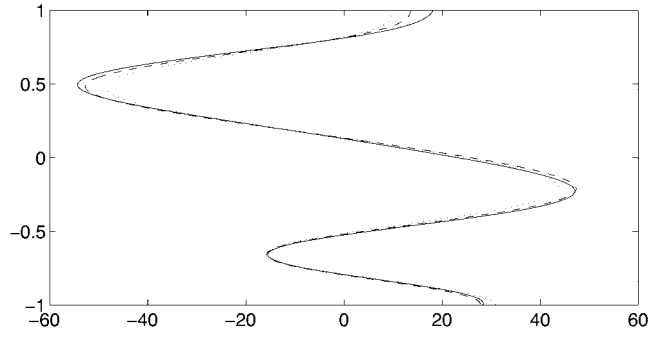

Fig. 3. The Limaye profile (solid) in the southern hemisphere band, and the zonally averaged velocity profiles for the equilibrium states with $\varepsilon = -0.02$ (dashed) and $\varepsilon = -0.035$ (dotted).

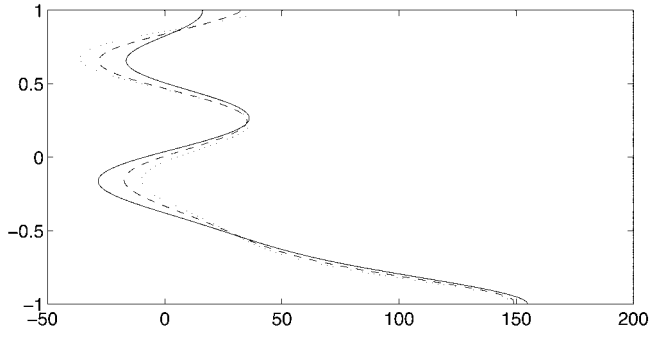

Fig. 5. The Limaye profile (solid) in the northern hemisphere band and the zonal velocity profiles for the equilibrium states with $\varepsilon = -0.02$ (dashed) and $\varepsilon = -0.032$ (dotted), and the same energy and circulation as the Limaye zonal flow; each of these computed solutions is purely zonal.

Concluding Discussion

The statistical theory developed here self-consistently produces equilibrium states possessing all three of the key properties *i*, *ii*, and *iii*. The results strongly suggest the use of such statistical equilibrium theories as inverse modeling tools to infer the statistical behavior of the small-scale motions from the observed large-scale structures. In the context of the one and one-half layer quasigeostrophic model used here, such an approach has shown that anticyclonic eddies dominate the small-scale fluctuations of potential vorticity. How consistent is this theoretical prediction of anticyclonic skewness with direct observations? Recent analysis of data from the Galileo mission (29) points to a source of intense anticyclonic small-scale forcing of the weather layer on Jupiter through moist convective towers—their significant horizontal divergence coupled with rotation leads to small-scale anticyclonic vorticity production. Also, numerical simulations of freely decaying shallow-water turbulence in a regime of balanced dynamics show a preponderance of anticyclones compared with cyclones (30). Careful numerical experiments with small-scale forcing could provide additional insight into this issue. At present, all observational and numerical evidence confirms the implication of the statistical equilibrium theory that the distribution of small-scale eddies is anticyclonically skewed.

The statistical equilibrium computations conducted here for midlatitude bands in the northern and southern hemispheres of Jupiter demonstrate that the structure of the zonal flow in the deep lower layer strongly influences whether or not coherent vortices emerge in the upper layer. By producing coherent vortices in the southern band, but not in the northern band, the results support Dowling's procedure (23) for inferring the deep lower layer flow from the observed zonal mean flow in the upper layer. Galileo data (31) showing that wind speed increases with depth below the weather layer independently confirms this procedure, which defines a lower layer flow that is faster than the upper layer flow. When an effective zonal topography is determined in this way, the large-scale zonal jet patterns and monopolar vortices observed in the Jovian weather layer are realized as equilibrium states of the statistical theory. Because these most probable states are stable with respect to both fine-grained fluctuations and coarse-grained perturbations, this characterization offers a theoretical explanation of the robustness of these observed flows. It would be interesting to apply the same methodology to wider bands on Jupiter and to other Jovian planets, and to compare the predictions of the theory with the diversity of behavior found on the giant planets.

The research of B.T. is partially supported by grants from the Department of Energy and the National Science Foundation. K.H. has been supported as a doctoral student through these grants. The research of A.M. is partially supported by grants from the National Science Foundation and the Office of Naval Research. M.D. has been supported as a postdoctoral fellow through these grants.

1. Dowling, T. E. (1995) *Annu. Rev. Fluid Mech.* **27,** 293–334.
2. Marcus, P. S. (1993) *Annu. Rev. Astrophys.* **31,** 523–573.
3. Rogers, J. H. (1995) *The Giant Planet Jupiter* (Cambridge Univ. Press, New York).
4. Turkington, B. (1999) *Commun. Pure Appl. Math.* **52,** 781–809.
5. DiBattista, M. T., Majda, A. J. & Turkington, B. (1998) *Geophys. Astrophys. Fluid Dyn.* **89,** 235–283.
6. Majda, A. J. & Wang, X. (2001) *Nonlinear Dynamics and Statistical Theories for Basic Geophysical Flows* (Lecture Notes at Courant Institute).
7. Pedlosky, J. (1979) *Geophysical Fluid Dynamics* (Springer, New York).
8. Dowling, T. E. & Ingersoll, A. P. (1989) *J. Atmos. Sci.* **46,** 3256–3278.
9. Salmon, R., Holloway, G. & Hendershott, M. C. (1976) *J. Fluid Mech.* **75,** 531–553.
10. Carnevale, G. F. & Frederiksen, J. S. (1987) *J. Fluid Mech.* **175,** 157–181.
11. Miller, J., Weichman, P. B. & Cross, M. C. (1992) *Phys. Rev. A* **45,** 2328–2359.
12. Robert, R. & Sommeria, J. (1991) *J. Fluid Mech.* **229,** 291–310.
13. Sommeria, J., Nore, C., Dumont, T. & Robert, R. (1991) *C. R. Acad. Sci. Ser. II* **312,** 999–1005.
14. Michel, J. & Robert, R. (1994) *J. Stat. Phys.* **77,** 645–666.
15. Ingersoll, A. P. & Cuong, P. G. (1981) *J. Atmos. Sci.* **38,** 2067–2076.
16. DiBattista, M. T., Majda, A. J. & Grote, M. (2001) *Physica D*, in press.
17. Grote, M. J. & Majda, A. J. (1997) *Phys. Fluids* **9,** 3431–3442.
18. Grote, M. J. & Majda, A. J. (2000) *Nonlinearity* **13,** 569–600.
19. Brands, H., Chavanis, P. H., Pasmanter, R. & Sommeria, J. (1999) *Phys. Fluids* **11,** 3465–3477.
20. DiBattista, M. T., Majda, A. J. (2000) *J. Phys. Oceanogr.* **30,** 1325–1353.
21. DiBattista, M. T., Majda, A. J. & Marshall, M. (2001) *J. Phys. Oceanogr.*, in press.
22. Limaye, S. S. (1986) *Icarus* **65,** 335–352.
23. Dowling, T. E. (1995) *Icarus* **117,** 439–442.
24. Turkington, B. & Whitaker, N. (1996) *SIAM J. Sci. Comput.* **17,** 1414–1433.
25. Arnold, V. I. (1982) *Mathematical Methods in Classical Mechanics* (Springer, New York).
26. Stamp, A. & Dowling, T. E. (1993) *J. Geophys. Res.* **98,** 847–855.
27. Bertsekas, D. P. (1982) *Constrained Optimization and Lagrange Multiplier Methods* (Academic, New York).
28. Ellis, R. S., Haven, K. & Turkington, B. (2001) *Nonlinearity*, in press.
29. Ingersoll, A. P., Geirasch, P. J., Banfield, D., Vasavada, A. R. & the Galileo Imaging Team. (2000) *Nature (London)* **403,** 630–632.
30. Polvani, L. M., McWilliams, J. C., Spall, M. A. & Ford, R. (1994) *Chaos* **4,** 177–186.
31. Atkinson, D. H., Ingersoll, A. P. & Seiff, A. (1997) *Nature (London)* **388,** 649–650.